J. Fluid Mech. (2024), *vol*. 999, A26, doi:10.1017/jfm.2024.970

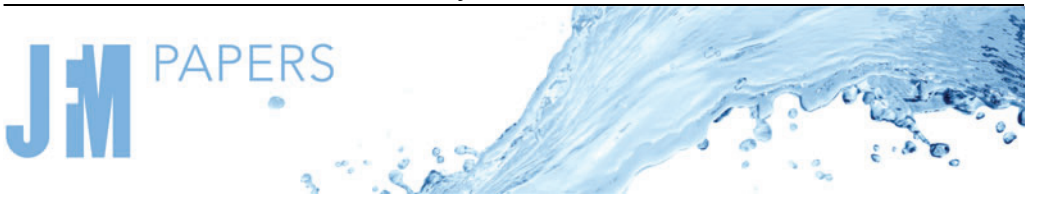

Towards a new roughness parametrization through the effective distribution function

F. Bruno[1],†, **S. Leonardi**[2] **and M. De Marchis**[3]

[1]Department of Architecture and Engineering, University of Enna "Kore", 94100 Enna, Italy

[2]Department of Mechanical Engineering, University of Texas at Dallas, 75080 Richardson, TX, USA

[3]Department of Engineering, University of Palermo, 90128 Palermo, Italy

(Received 13 March 2024; revised 20 September 2024; accepted 5 October 2024)

Turbulent flows over rough surfaces can be encountered in a wide range of engineering applications. Despite the progress made after several decades of studies, the prediction of drag and roughness function from the surface geometrical parameters remains an open question. Several methods have shown encouraging results. However, they lack generality and present some scatter in the data. In this paper we propose a new parameter, the effective distribution (*ED*), which lays foundation on the effective slope with some changes to take into account the sheltering effect of large roughness elements and the drag induced by pinnacles higher than the average roughness elements. To develop this new correlation between geometrical features of the wall and the drag, we performed a set of simulations of the turbulent flow over a rough surface made of triangular elements varying their height and spatial distribution. The *ED* correlates quite well both with the drag and the roughness function for a wide range of cases having different mean roughness height, skewness and kurtosis. To further validate the *ED*, and assessing how it can be generalized to real rough wall, an irregular wall made from the superposition of random sinusoidal function was considered. Results were consistent with the correlation here presented.

Key words: turbulence simulation, turbulent boundary layers

1. Introduction

Rough surfaces are encountered in a wide range of engineering and environmental applications. The flow in heat exchangers, the atmospheric boundary layer over urban areas, complex topography or vegetation and the leading-edge erosion of turbine blades are just a few examples of the wide range of problems where roughness plays a key role.

† Email address for correspondence: federica.bruno@unikore.it

Roughness in general leads to a drop in system performance and a huge boost in the management costs. Hence, predicting the effect of rough walls on turbulence has become an important design prerequisite for practical applications. Starting from the seminal work of Nikuradse (1933), in the last decades, several studies have been carried out to understand the flows physics over corrugated walls. Despite extensive efforts being made by the scientific community, our knowledge cannot be considered sufficiently robust and universal. One of the first attempts to predict the main roughness effect was given by Hama (1954), introducing the correlation between a geometrical parameter, known as equivalent sand grain roughness k_s (Schlichting 1937), and the energy loss induced by the roughness. Hama (1954) observed that the main effect of the roughness is the downward shift of the mean velocity profile (scaled in inner units) in the log region, known as roughness function ΔU^+. Hereafter, the superscript $^+$ denotes variables made non-dimensional with inner variables $u_\tau = (\tau_s/\rho)^{(0.5)}$ and ν/u_τ, where u_τ is the friction velocity, ρ is the fluid density, ν is the kinematic viscosity and τ_s is the wall shear, equal to the sum of the viscous (or skin frictional) stress $\overline{C_f} = (1/L_x)\int_0^{L_x}(\mu\partial\langle U^*\rangle/\partial y^*)(1/\rho U_c^2)\,\mathrm{d}s$ and the form drag $\overline{P_d} = (1/L_x)\int_0^{L_x}\langle P\rangle \boldsymbol{n}\cdot\boldsymbol{x}\,\mathrm{d}s$, ($\boldsymbol{n}$ is the normal to the surface, $\boldsymbol{x}$ is the unit vector in the streamwise direction and s is a coordinate along the surface). The symbol $\langle\cdot\rangle$ indicates quantities averaged in the spanwise direction and time, * indicates dimensional units and L_x represents the streamwise length. The original formulation to calculate the roughness function was given by Hama (1954), who introduced the following correlation:

$$\Delta U^+ = \frac{1}{\kappa}\ln(k_s^+) + B, \tag{1.1}$$

where κ is the von Kármán constant, $k_s^+ = k_s{\cdot}u_\tau/\nu$ and B is a constant. Unfortunately, for a general rough wall, k_s cannot be calculated *a priori*; it can be, in fact, determined once the mean velocity profile is known. In fact, as pointed out by several authors (see among others Flack, Schultz & Volino (2020)), k_s is not a physical measure of the corrugation. The prediction of the drag, as well as ΔU^+, based on geometrical features of the wall, has received extensive attention in the past and a variety of roughness correlations have been developed in the literature (see among others Sigal & Danberg (1990), Waigh & Kind (1998), Van Rij, Belnap & Ligrani (2002), Bons (2005), Flack & Schultz (2010), Chan *et al.* (2015), Busse, Thakkar & Sandham (2017), Forooghi *et al.* (2017), Thakkar, Busse & Sandham (2017), Piomelli (2019), De Marchis *et al.* (2020) and Chung *et al.* (2021)). Several parameters were analysed in the past, for instance the mean roughness height k^+, the peak-to-valley distance k_{pv}^+, the root mean square k_{rms}^+, the roughness solidity λ, the skewness S_k, the kurtosis K_s and the effective slope (ES), using both experiments or numerical simulations over two-dimensional (2-D) or three-dimensional (3-D) roughness. Schlichting (1937) introduced the term roughness solidity (λ) to quantifies the roughness density and is defined as the total projected frontal roughness area per unit wall-parallel projected area. It has been observed that the roughness function ΔU^+ increases with density up to $\lambda = 0.15$, where it is maximum, and then decreases for larger λ (Jiménez 2004; Flack & Schultz 2014). This indicates qualitatively that increasing the roughness density while in the sparse regime ($\lambda < 0.15$) increases the drag due to the increased frontal area of the roughness. In the dense regime ($\lambda > 0.15$), mutual sheltering of roughness elements leads to a decrease in drag as the density is increased (Macdonald, Griffiths & Hall 1998; Oke 1988; Jiménez 2004). Despite the utilization of solidity for distinguishing between different roughness types, it cannot solely fully characterize a rough surface. For example, Jiménez (2004) showed a dependency on λ^{-2}, while λ^{-5} has

been proposed by Dvorak (1969). Other geometrical parameters are required to describe the mutual sheltering of the roughness elements. The effective slope, ES, is connected to the solidity parameter, λ, through the relation $ES = 2\lambda$ (Napoli, Armenio & De Marchis 2008; MacDonald *et al.* 2016; Thakkar *et al.* 2017). MacDonald *et al.* (2016) showed that the value of $ES \approx 0.35$, defined as a demarcation point between waviness regime ($ES < 0.35$) and roughness regime ($ES > 0.35$), is associated with a solidity value of $\lambda = 0.175$. Moreover, Mejia-Alvarez & Christensen (2013) and De Marchis (2016) have reported that $ES = 0.35$ is a limit between slope dependent and height dependent flows. Furthermore, some studies focused the attention on regular elements arranged over a flat plate (see among others Leonardi *et al.* (2003), Volino, Schultz & Flack (2011), De Marchis (2016), Gatti *et al.* (2020), Modesti *et al.* (2021) and Busse & Zhdanov (2022) for 2-D elements, and Orlandi & Leonardi (2008), Boppana, Xie & Castro (2010), Hong, Katz & Schultz (2011) and Busse & Jelly (2020) for 3-D elements). Recently, Millward-Hopkins *et al.* (2011) and Yang *et al.* (2016) have formulated drag-prediction models that use a sheltering argument to account for the interaction between roughness elements. Geometrical statistics, developed so far, correlate well with the drag of some particular type of roughness but lack universality with other generic irregular walls. This calls for an effort to develop a universal correlation to predict roughness effects. In this study, direct numerical simulations have been performed to reveal the flow features around rough elements. A new parameter, called effective distribution (ED), has been introduced. The ED is based on a modified version of the ES (Napoli *et al.* 2008) and the proposed results show a good correlation with different roughness shape. The paper is organized as follows: § 2 describes the numerical procedure adopted for direct numerical simulations, § 3 highlights flow configurations, results are presented in § 4 and conclusions are drawn in § 5.

2. Numerical procedure

Direct numerical simulations have been performed for a fully developed turbulent channel flow with roughness on the bottom wall. The non-dimensional Navier–Stokes and continuity equations for incompressible, neutrally stable flows can be expressed as

$$\frac{\partial U_i}{\partial t} + \frac{\partial U_i U_j}{\partial x_j} = -\frac{\partial P}{\partial x_i} + \frac{1}{Re}\frac{\partial^2 U_i}{\partial x_j^2} + \Pi\delta_{i1}, \tag{2.1}$$

$$\boldsymbol{\nabla}\cdot\boldsymbol{U} = 0, \tag{2.2}$$

where Re is the Reynolds number based on the bulk velocity ($U_b = 1/h\int_0^h U\,\mathrm{d}y$), which is held constant in time, h is the channel half-height, δ_{ij} is the Kronecker delta, U_i is the ith component of the velocity vector, x_i is the ith coordinate direction and P is the pressure. The quantity Π is the pressure gradient which varies with time in order to keep the flow rate constant. The Navier–Stokes equations were discretized in an orthogonal coordinate system using the staggered central second-order finite difference approximation. The surface roughness was treated using the immersed boundary technique, which allows solution over complex geometries without the need for intensive body-fitted grids. It consists of imposing $U_i = 0$ on the body surface, which does not necessary coincide with the grid. Full details about the immersed boundary method and the numerical schemes can be found in Orlandi & Leonardi (2006).

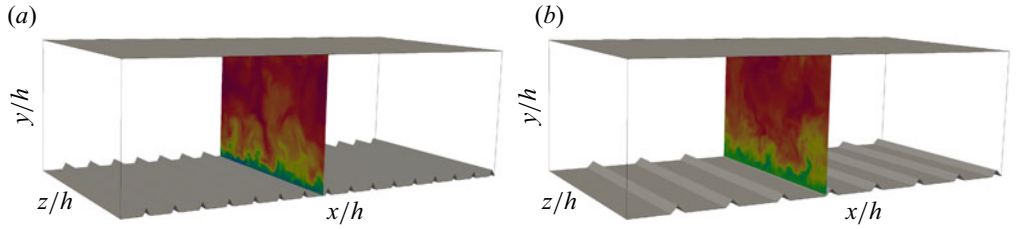

Figure 1. The 3-D computational domain for the two set of rough surfaces considered: (*a*) set 1 having 16 triangles and $k/h \approx 0.1$; (*b*) set 2 having eight triangles and $k/h \approx 0.2$.

Marker	Sketch	Case	L_x	L_y	L_z	Re_τ	Δx^+	Δy^+_{min}	Δy^+_{max}	Δz^+
♦		Flat	$12.8h$	$2.2h$	πh	240	11.93	1.19	11.26	5.85
□		$A1_1$	$6.4h$	$2.2h$	πh	458	5.73	0.92	11.92	3.94
△		$B1_1$	$6.4h$	$2.2h$	πh	558	6.97	1.12	14.51	4.80
△		$B2_1$	$6.4h$	$2.2h$	πh	568	7.09	1.14	14.76	4.88
○		$C1_1$	$6.4h$	$2.2h$	πh	510	6.38	1.02	13.27	4.39
○		$C2_1$	$6.4h$	$2.2h$	πh	538	6.72	1.08	13.98	4.62
○		$C3_1$	$6.4h$	$2.2h$	πh	581	7.27	1.16	15.11	4.99
○		$C4_1$	$6.4h$	$2.2h$	πh	589	7.36	1.18	15.31	5.06
□		$A0$	$6.4h$	$2.2h$	πh	465	5.81	0.93	12.09	4.00
□		$A1_2$	$6.4h$	$2.2h$	πh	567	7.09	1.13	14.75	4.88
□		$A1_{2b}$	$6.4h$	$2.2h$	πh	589	7.37	1.18	15.32	5.07
△		$B1_2$	$6.4h$	$2.2h$	πh	703	8.79	1.41	18.29	6.04
△		$B2_{2b}$	$6.4h$	$2.2h$	πh	791	9.88	1.58	20.56	6.80
○		$C1_2$	$6.4h$	$2.2h$	πh	645	8.06	1.29	16.77	5.54
○		$C2_2$	$6.4h$	$2.2h$	πh	675	8.43	1.35	17.54	5.80
○		$C3_2$	$6.4h$	$2.2h$	πh	731	9.14	1.46	19.01	6.28
○		$C4_2$	$6.4h$	$2.2h$	πh	742	9.27	1.48	19.28	6.37

Table 1. Legend, sketch of the geometrical shape, computational box and grid resolution of the different walls studied here.

3. Flow configuration

Periodic boundary conditions have been applied in the streamwise (x or x_1) and spanwise (z or x_3) directions while a no-slip condition has been imposed in the wall-normal direction (y or x_2). The computational box in the x, y, z direction is $6.4h \times 2.2h \times \pi h$, respectively; a sketch of two of the roughness cases considered here is shown in figure 1. The computational domain has been discretized using $512 \times 256 \times 256$ grid points. The mesh is uniform in the streamwise and spanwise directions, with $\Delta x/h = 0.0125$ and $\Delta z/h = 0.009$. On the other hand, a non-uniform mesh has been used in the y direction. Specifically, in the wall-normal direction the points are clustered near the wall within the cavity $\Delta y_{min}/h = 0.002$. The mesh increases towards the channel centreline, with $\Delta y_{max}/h = 0.026$. The Reynolds number is $Re = 4300$ and corresponds to the friction Reynolds number $Re_\tau = 240$ when both walls are smooth. Details of the computational box and resolution are summarized in table 1.

For a fixed pitch to height ratio $w/k = 4$, which is below the value for which transverse bars can be considered virtually isolated ($w/k = 8$, Leonardi *et al.* (2003)), two sets of simulations have been analysed varying the roughness height. The first set is made of 16 triangular transverse bars equally spaced in the streamwise direction $w/h = 0.4$

Marker	Sketch	Case	k/h	k_{max}/h	w/h	λ/h	ES	ED	K_u	S_k	$D/\rho U_b^2$	ΔU^+
♦		Flat	0.00	0.00	0.00	0.00	0.00	0.00	0.00	0.00	0.12	0.30
■		$A1_1$	0.10	0.00	0.40	0.00	0.50	0.57	7.49	2.64	0.23	11.50
▲		$B1_1$	0.10	0.20	0.40	3.20	0.56	0.67	11.38	3.07	0.34	13.00
▲		$B2_1$	0.10	0.20	0.40	3.20	0.50	0.69	13.17	3.30	0.35	13.00
●		$C1_1$	0.09	0.18	0.40	0.40	0.56	0.66	11.61	3.13	0.28	12.20
●		$C2_1$	0.09	0.18	0.40	0.80	0.56	0.69	11.61	3.13	0.31	12.80
●		$C3_1$	0.09	0.18	0.40	1.20	0.56	0.71	11.61	3.13	0.37	13.50
●		$C4_1$	0.09	0.18	0.40	1.60	0.56	0.73	11.61	3.13	0.38	13.80
■		$A0$	0.20	0.00	6.40	0.00	0.06	0.25	7.49	2.64	0.23	11.00
■		$A1_2$	0.20	0.00	0.80	0.00	0.50	0.65	7.49	2.64	0.35	13.50
■		$A1_{2b}$	0.22	0.00	0.80	0.0	0.55	0.72	7.49	2.64	0.38	13.60
▲		$B1_2$	0.20	0.40	0.80	6.40	0.56	0.77	11.38	3.07	0.52	14.60
▲		$B2_2$	0.20	0.40	0.80	6.40	0.50	0.79	13.17	3.30	0.55	14.60
▲		$B2_{2b}$	0.23	0.46	0.80	6.40	0.58	0.91	13.17	3.30	0.68	15.50
●		$C1_2$	0.18	0.36	0.80	0.80	0.56	0.76	11.61	3.13	0.45	13.70
●		$C2_2$	0.18	0.36	0.80	1.60	0.56	0.78	11.61	3.13	0.49	14.20
●		$C3_2$	0.18	0.36	0.80	2.40	0.56	0.81	11.61	3.13	0.58	15.00
●		$C4_2$	0.18	0.36	0.80	3.20	0.56	0.83	11.61	3.13	0.60	15.00

Table 2. Geometrical and flow properties: k/h, roughness height; k_{max}/h, big element roughness height (equal to $2{*}k/h$); w, cavity width; λ, distance between big elements; ES, effective slope; ED, effective distribution; K_u, kurtosis; S_k, skewness; $D/\rho U_b^2$, total drag; ΔU^+, roughness function.

(figure 1*a*). The baseline case (■ case $A1_1$), has a constant roughness height $k/h = 0.1$. In the second set of simulations (figure 1*b*), we halved the number of triangular bars in streamwise direction but doubled the roughness height to $k/h = 0.2$ (■ case $A1_2$). The subscript indicates the roughness height. Other cases are considered as a modification of the baseline to highlight specific geometrical features, such as a protuberance above the roughness layer and the wake of larger elements affecting the downstream roughness. The height is slightly adjusted in each case to keep constant either the value of ES, kurtosis and skewness. In cases $B1_1$ (▲) and $B1_2$ (▲) we doubled the vertical size of one element; in cases $B2_1$ (▲), $B2_2$ (▲) and $B2_{2b}$ (▲) we removed the element immediately downstream of the tallest one. The set of simulations labelled with C present two taller triangles, with streamwise distances gradually increasing from $C1_1$ to $C4_1$ (●, ●, ●, ●) and from $C1_2$ to $C4_2$ (●, ●, ●, ●). The geometrical and flow properties are summarized in table 2. According to the values of the friction Reynolds number and k/h here considered, a fully rough regime is ensured (see among others Bandyopadhyay (1987) and Leonardi, Orlandi & Antonia (2007)).

4. Results and discussion

The effect of the roughness is to shift downward the mean velocity U^+ profile, with respect to that on a smooth wall, by an increment ΔU^+, i.e.

$$U^+ = \kappa^{-1} \ln y^+ + C - \Delta U^+. \tag{4.1}$$

The roughness function in the present paper has been computed as the distance of the log region with respect to the ideal smooth wall with $C = 5.6$. The friction velocity on the rough wall is computed as the sum of the form drag and frictional drag so there are no uncertainties due to the asymmetry of the channel. The velocity profiles on the upper smooth wall (not shown here because beyond the scope of the paper), when scaled with

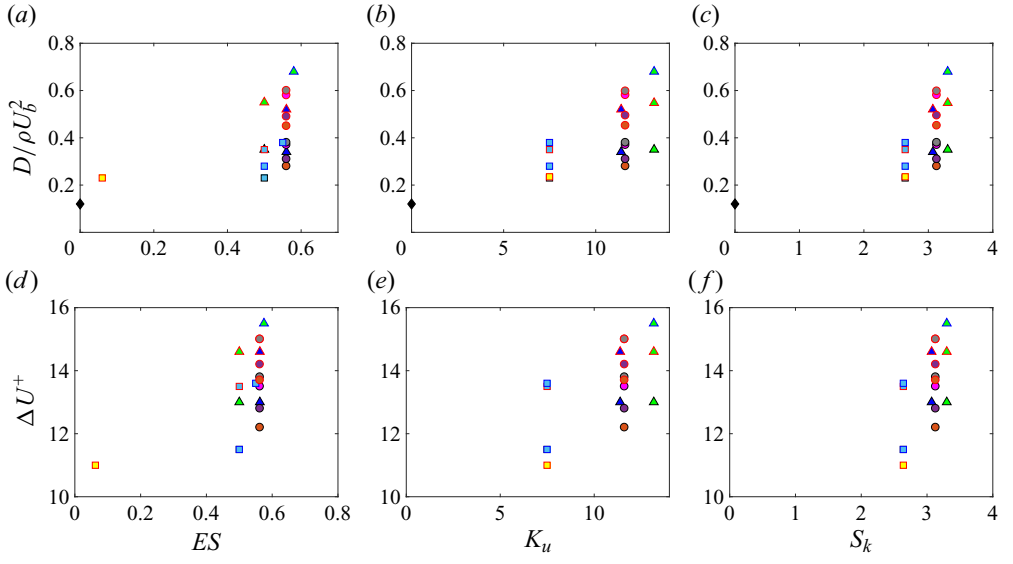

Figure 2. Drag and roughness function dependence on the geometrical features of the rough wall (*ES*, skewness and kurtosis). Symbols as in table 1.

the proper friction velocity (from the shear on that wall and not from the pressure drop) agree well with the law of the wall although the extent of the log region is shorter due to the smaller local turbulent Reynolds number. The virtual origin in y is chosen to have a slope of $\kappa = 0.41$. Other choices could have been made for the virtual origin, but since the goal here is to calculate the roughness function for a large number of different cases, fixing the slope of the log region to κ^{-1} allowed a consistent calculation of the roughness function. In figure 2 the total drag and the roughness function are plotted as function of the *ES*, skewness and kurtosis. For the same *ES*, or K_u or S_k, the drag varies significantly, up to 300 % and the roughness function up to 40 %. The value of the drag has been included in the analysis because it does not present the uncertainties that the roughness function has in its definition (virtual origin, the slope of the log region and the value of the constant C). Even grouping data relative to the same mean roughness height or root mean square does not eliminate the scatter in the data.

4.1. *Inconsistency in geometrical parametrization*

The flow structure and the pressure around the roughness elements have been analysed to understand why the drag and roughness function vary despite having the same geometrical statistics (mean roughness height, *ES*, S_k or K_u). In particular, comparing $A1_1$ (■ uniform triangles) and $B1_1$ cases, (▲ same as $A1_1$ with an element Δk higher), with a slight change of *ES* corresponds to a major difference in drag. For uniform roughness, the cavities are filled with a recirculating flow (figure 3*a*). The non-dimensional form drag (normalized with ρU_b^2) of each element is $P_d = 0.005$. On the other hand, in $B1_1$, the streamlines impinge on the tallest element (the element '0' in figure 3*b*) generating a stagnation point and high-pressure differences with respect to the leeward side of the wedge. The form drag is $P_d = 0.04$, approximately eight times larger than that of uniform triangles. This shows how sensitive the drag is to pinnacles emerging outside the roughness layer, which,

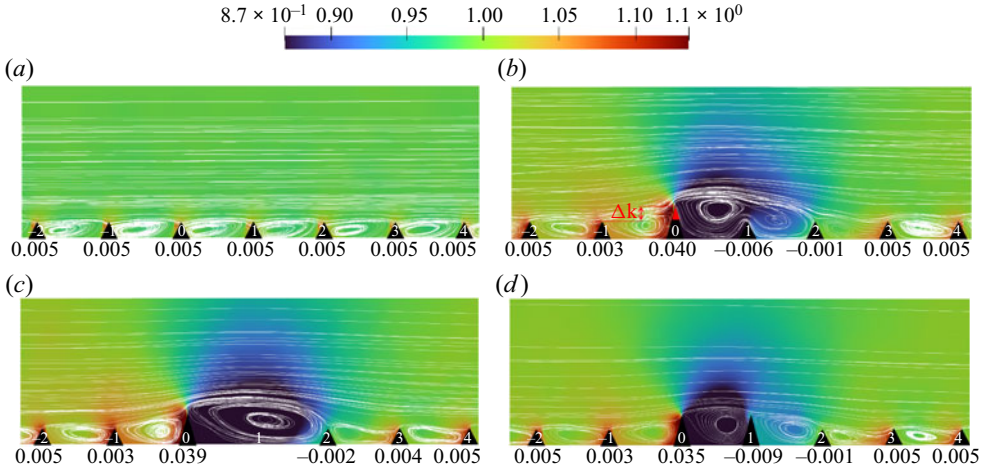

Figure 3. Streamlines superposed to colour contours of pressure: (*a*) $A1_1$ (■); (*b*) $B1_1$ (▲); (*c*) $B2_1$ (▲); (*d*) $C1_1$ (●). The pressure drag of each triangle is indicated below them, i.e. $P_d(4) = 0.005$. Definition of Δk is included in the figure.

instead, is not accounted for in *ES*, skewness and kurtosis. The form drag of the upstream triangle (labelled '−1') is slightly smaller because the streamlines are tilted upward by the taller element. The large recirculation closes on the second element downstream (labelled '2') at a distance of approximately $8k$. The pressure drag of the two roughness elements in the wake is very small and negative, meaning that the pressure on the leeward side is higher than that on the windward side. The drag of the other roughness elements is to a good approximation unaffected implying that a perturbation to the geometrical topography of the surface affects the flow slightly upstream (up to $4k$) and a bit more downstream ($8k$). The surface $B2_1$ is obtained by removing the triangle (labelled '1' in figure 3*b*) downstream of the highest roughness element. The mean streamlines are very similar with a main recirculation originated on the highest peak and closing approximately $8k$ downstream (figure 3*c*). The drag on each element is approximately the same. The overall drag and roughness function are to a good approximation the same as those of $B1_1$ despite variations of *ES* and K_u. This suggests that roughness elements located in the wake region of higher elements must be weighted differently in the geometrical statistics of the surface. Adding a second taller roughness element to $B1_1$, immediately downstream (labelled '1' in figure 3*d*), surface $C1_1$, increases the mean surface height, as well as the higher moments statistics, but reduces the drag (and roughness function) instead of increasing it (as it would have been expected by having a higher mean roughness). The wake of the first higher pinnacle shields the second, as already considered in various prior studies (see among others Raupach, Antonia & Rajagopalan (1991), Shao & Yang (2005), Shao & Yang (2008) and Yang *et al.* (2016)). These studies denoted, as volumetric sheltering, the momentum reduction in the wakes of roughness elements and its effect on the drag of neighbouring roughness elements. The recirculation shrinks compared with $B1_1$ and $B1_2$, filling the cavity formed by the two higher triangles (elements '0' and '1' of figure 3*d*). Increasing the distance between the two highest pinnacles (cases $C3_1$ ● and $C4_1$ ●, figure 4*a*,*b*), leads to an increase of drag and ΔU^+ because the streamlines tend to reattach on the lower array of triangles with a consequent increase of pressure drag on the large element. These results suggest that the position of the roughness elements, affects the flow physics and the drag

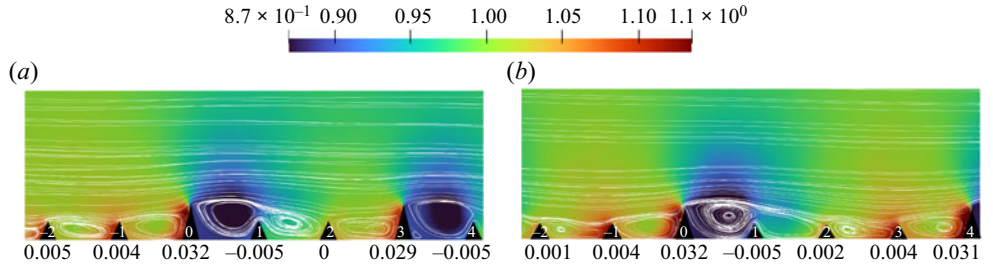

Figure 4. Streamlines superposed to colour contours of pressure: (*a*) $C3_1$ (●); (*b*) $C4_1$ (●).

despite the geometrical feature K_u or S_k are the same. A single pinnacle much higher than the others has a major effect on the flow. Its contribution is not proportional to the wet area, or exposed area to the flow; it is much higher if the upstream elements are smaller. It could be interpreted mathematically into a geometry height gradient, which was partially taken into account by the *ES*. However, cases $C1_1$–$C4_1$ highlight how it is important the presence of other tall roughness elements upstream, and their wake. The distance between two consecutive highest peaks is a key parameter to determine the influence of roughness on turbulent flow.

4.2. *Effective distribution*

The analysis of § 4.1 showed that any parametrization based on geometrical features of the walls needs to be consistent with the following points.

(i) The roughness elements in the wake of larger elements have a negligible contribution to the drag. As a consequence, the geometrical quantities used to parameterize the roughness should be filtered by the contribution of those elements in the wake length.

(ii) The contribution to the drag of each roughness element depends on its pattern and distance from previous elements (figure 3*b*).

(iii) The distance between two consecutive rough elements affects the velocity distribution, the momentum in the cavity and as a consequence the intensity of the stagnation point on the windward roughness element.

These features have been included in a new geometrical parametrization, *ED*, as a revision of the *ES* introduced by Napoli *et al.* (2008), as follows:

$$\begin{cases} ED = \left(ES - \displaystyle\sum_{j=1}^{m}\sum_{i=1}^{n} \alpha_{i,j} \cdot ES_i + \sum_{j=1}^{m}\sum_{i=1}^{m} \beta_{i,j} \cdot ES_{\Delta k_i} \right) + \sum_{i=1}^{n} \frac{w_{i,i+1}}{L_x} \frac{k}{\delta_k} \\ \alpha_{i,j} = \min\left(1, \dfrac{\Delta k_j}{w_{i,j}}\right) \quad \text{for } 1 \leqslant \dfrac{w_{i,j}}{k} < 8, \quad \alpha_{i,j} = 0 \quad \text{for } \dfrac{w_{i,j}}{k} > 8 \\ \beta_{i,j} = \dfrac{\lambda_{i,j}}{wake_j} \quad \text{for } \dfrac{\lambda_{i,j}}{wake_j} < 1, \quad \beta_{i,j} = 1 \quad \text{for } \dfrac{\lambda_{i,j}}{wake_j} > 1 \end{cases} \tag{4.2}$$

where *ES* is the overall *ES* calculated as in the original formulation of Napoli *et al.* (2008) ($(1/L_{x_1}) \int_{L_{x_1}} |\partial k(x_1)/\partial x_1| \, \mathrm{d}x_1$), ES_i is the *ES* of the *i*th element, weighted by

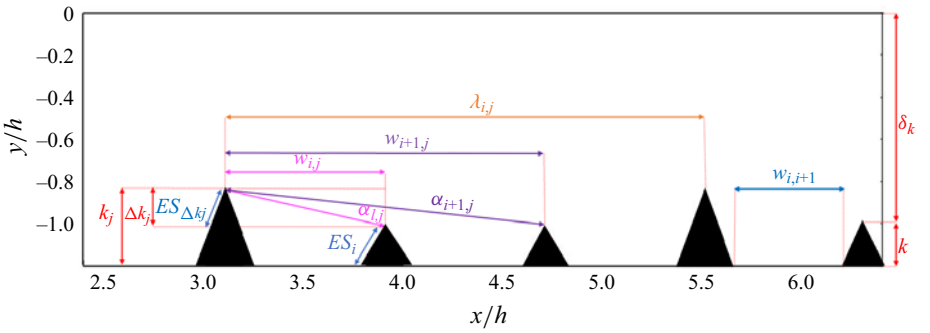

Figure 5. Schematic representation of the parameter defined in the determination of the *ED*.

$\alpha_{i,j} = \min(1, \Delta k_j/w_{i,j})$ with $w_{i,j}$ the distance between the jth higher peak, emerging Δk_j over the crest plane, and the ith roughness element. The index n in the summations indicates the number of roughness elements while m is the number of pinnacles above the crests plane. The second term on the right-hand side of (4.2) subtracts from the *ES* the contribution of the elements in the wake of the higher peaks. The coefficient $\alpha_{i,j}$ takes into account the effect of the wake of the jth pinnacle above the crests plane on the ith roughness element. This term is unity when the ith roughness element is close to the higher peak 'j' and in its wake, and decreases to zero as it is farther apart from it. In fact, when the cavity between two roughness elements is narrow, the flow has a d-type behaviour and the drag is almost unaffected by that roughness element so its contribution to the *ES* is removed. By increasing $w_{i,j}$, the distance of the roughness element from the peak, its contribution to the drag gradually increases and then just a fraction of its *ES* is subtracted from the overall *ES*. Previous papers showed that for a pitch to height ratio larger than 8 the roughness elements act as isolated with a reattachment of the flow on the flat wall of the cavities. Therefore the wake length can be approximated to $wake_j = 8k_j$, which is this dataset could be simplified to $wake_j = 8k_{max}$ since all the pinnacles above the crests plane have the same height. However, to keep a general formulation of (4.2) $wake_j = 8k_j$ is used allowing to have a non-uniform distribution of elements above the crests plane. For $w_{i,j}/k_j > 8$ (resulting in $w_{i,j} > wake_j$), indicating the roughness element outside the wake region, $\alpha_{i,j} = 0$. A similar concept is used to account for the pattern of the higher pinnacles, the m elements emerging above the crests plane. When the downstream pinnacle is too close to that upstream, its contribution to the drag is smaller than when it is isolated. Therefore, the $ES_{\Delta k_j}$ is weighted by $\beta_{i,j} = \lambda_{i,j}/wake_j$, where $\lambda_{i,j}$ is the distance between the pinnacles i and j that are higher than the crests plane. When $\lambda_{i,j} < wake_j$, the downstream pinnacle is in the wake region of the upstream pinnacle. This means that the flow around the downstream pinnacle (i) will be affected by the wake of the upstream pinnacle (j), which results in a reduced contribution to the overall drag. To account for this effect, a coefficient β is introduced, which scales the contribution of the downstream pinnacle to the overall drag. When $\lambda_{i,j} < wake_j$, $\beta_{i,j}$ is less than 1 to reflect the reduced contribution of the downstream pinnacle. As $\lambda_{i,j}$ increases and the downstream pinnacle (i) moves out of the wake region, $\beta_{i,j}$ increases as well, until it reaches a constant value of 1 when $\lambda_{i,j} > wake_j$. This indicates that both pinnacles have the same contribution to the overall drag and can be treated as isolated peaks. In figure 5 a sketch of these distances is depicted. The fourth term in (4.2) accounts for the distance between two consecutive roughness elements which, as observed by Leonardi *et al.* (2003), affects the velocity profile, stagnation pressure and then the drag. By definition, the *ES* does not take into

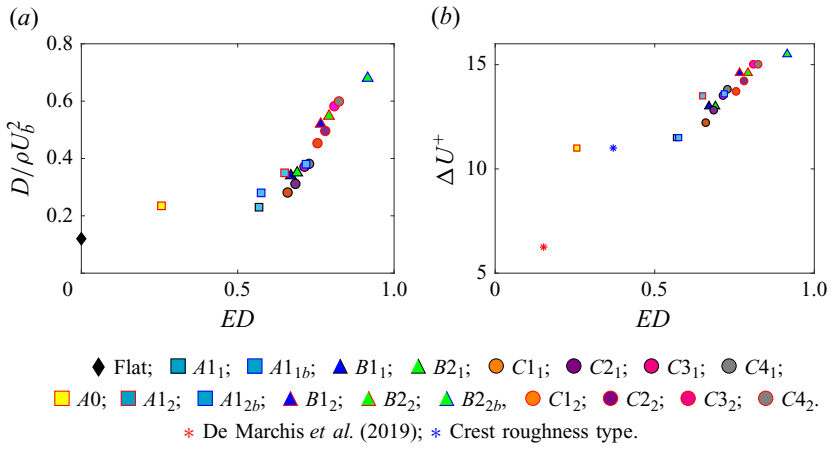

Figure 6. Drag and roughness function as function of the *ED*.

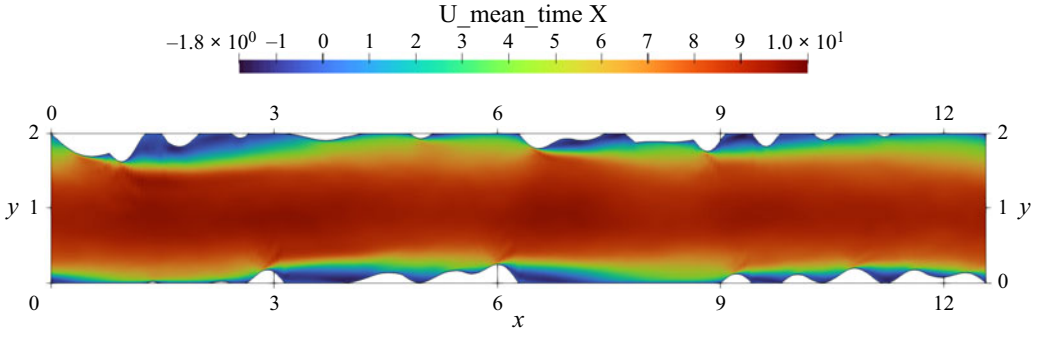

Figure 7. Contour plot of the mean streamwise velocity for the irregular rough wall of De Marchis *et al.* (2019).

account how wide are the cavities between roughness elements; it is, in fact, calculated only in the domain region characterized by roughness elements, *ES* being zero everywhere else. Nevertheless, looking at the streamlines depicted in figure 4, the distance between two consecutive elements $w_{i,i+1}$ has considerable effect on the fluid flow, showing the importance to taking into account these features. The dependence on the scale of roughness is accounted for with k/δ_k, where δ_k is the outer layer length scale (channel half-height or boundary layer thickness). In the present research two roughness heights were simulated, thus further geometrical configurations are required to confirm the role of the fourth term of (4.2). Figure 6 shows the correlation between the *ED* and the total drag or roughness function. The novel parametrization proposed in this paper, *ED*, correlates with the drag significantly better than the *ES* (shown in figure 2). A large variation in terms of drag and roughness function for the same value of *ES* was observed in figure 2, suggesting that the *ES* alone may not fully capture the impact of geometrical features on turbulent flows. On the other hand, the *ED*, taking into account the geometrical features which affect the turbulent flows discussed above, varies smoothly with the drag and roughness function. To further corroborate our previous finding and validate the *ED*, we applied it to a more complex irregular rough wall (figure 7). The irregular surface shape was generated through the superimposition of sinusoidal functions with random amplitudes and four different

wavelengths, see De Marchis, Milici & Napoli (2019). To use the *ED*, it is necessary to define a crests plane and then the pinnacles emerging above it. While this is obvious in the simplified cases discussed before, it is not straightforward for a more generic surface with peaks of variable height as that in (figure 7). The method we used consists in identifying the local peaks of the surface and then calculating the probability density function of those values using a number of bins equal to one third of the samples to have some statistical convergence. The crests plane was taken as the most probable peak height. The calculation of the distances between peaks, and the *ED* is then straightforward. Since the value of *ED* of the original case in De Marchis *et al.* (2019) was very small, the mean roughness height was increased to have a higher value of the *ED*. Specifically, the new geometry (reported as 'crest roughness type' using the '$*$' marker in the caption of figure 6) has a value of $ED = 0.37$ quite similar to the range here analysed. Data from both cases have been included in figure 6(*b*). Despite the surface in De Marchis *et al.* (2019) not being used to develop (4.2) but used as an independent validation only, results are consistent with the correlation between *ED* and roughness function obtained with our database of triangular roughness elements. This result suggests that the *ED* has the potential to be generalized to more complex and realistic 2-D geometries. More work is needed to extend it to 3-D roughness.

5. Conclusions

Direct numerical simulations have been performed to analyse a set of 2-D rough surfaces using triangle-shaped elements. One of the main challenges of the last decade was the prediction of a drag and roughness function based on surface topography, which requires a parametrization. Therefore, 17 geometries with different shapes but similar *ES*, skewness and kurtosis have been investigated. The study found that for most of the data, different shapes with the same geometrical quantities can result in different drag and roughness functions. To address this issue, a new geometrical parameter, called *ED*, was introduced. The *ED* is a geometrical parameter that accounts for the physical behaviour of the fluid around roughness elements. It is calculated based on flow features typically occurring in rough flow. The first suggested that roughness in the wake of large pinnacles has a negligible contribution to the drag and should not be included in the calculation of geometrical statistics of the surface to predict the drag. In addition, *ED* recognizes that roughness elements have contributions to the drag and ΔU^+ based on their size and pattern. The *ED* has been calculated as a modification to the *ES*, by subtracting the contribution of roughness elements located in the wake region and adding the contribution of pinnacles above the crest plane. Additionally, if the surface is characterized by more than a peak emerging above the crests plane, the distance between two subsequent pinnacles has to be considered. When the downstream pinnacle is in the wake region of the upstream pinnacle its contribution to the drag and then to the calculation of *ED* is reduced. On the other hand, as the separation increases and the downstream pinnacle moves out of the wake region, it is no longer influenced by the flow dynamics of the upstream pinnacle, and can be treated as an isolated peak. The *ES* lacks details regarding the separation between individual elements, particularly evident in a flat section where *ES* equals zero. As pointed out by Leonardi *et al.* (2003), the velocity profile undergoes significant influence from the flat section located downstream of each element. To address the influence of the flat section, the final term in (4.2) was incorporated. Overall, the *ED* provides a representative geometrical parameter of the entire roughness configuration, taking into account the peaks above the mean roughness, the wake region induced by

the higher elements, and the distance between two consecutive elements. The *ED* was shown to correlate well with drag and roughness function for the large dataset used to develop it as well as for a more realistic irregular rough wall generated with random sinusoidal functions. Overall, the *ED* improves previous correlations between the drag and geometrical features of the wall. More work is still required to further generalize it to roughness surfaces irregular in the spanwise direction.

Funding. The authors greatly appreciate the financial support provided by the following projects. S.L. and F.B. were partially supported by National Science Foundation grant no. 2202710. RETURN Extended Partnership and received funding from the European Union Next-GenerationEU (National Recovery and Resilience Plan – NRRP, Mission 4, Component 2, Investment 1.3 – D.D. 1243 2/8/2022, E0000005). The Texas Advanced Computing Center, and High Performance Computing at UT Dallas are acknowledged for providing computational time. TiSento – SENSORIALIZED COMPOSITE PIPE FOR HYDRAULIC APPLICATIONS, n. 084221000550 CUP G18I18001710007. Funded under measure 1.1.5 of the PO FESR SICILY 2014-2020. This research has been partially supported by the European Union – NextGenerationEU – National Sustainable Mobility Center CN00000023, Italian Ministry of University and Research Decree n. 1033–17/06/2022, Spoke 3, CUP B73C22000760001.

Declaration of interests. The authors report no conflict of interest.

Author ORCIDs.
F. Bruno https://orcid.org/0000-0002-4037-4790;
S. Leonardi https://orcid.org/0000-0002-4570-2255;
M. De Marchis https://orcid.org/0000-0002-3093-3245.

References

BANDYOPADHYAY, P.R. 1987 Rough-wall turbulent boundary layers in the transition regime. *J. Fluid Mech.* **180**, 231–266.

BONS, J. 2005 A critical assessment of Reynolds analogy for turbine flows. *Trans. ASME J. Heat Transfer* **127** (5), 472–485.

BOPPANA, V.B.L., XIE, Z.-T. & CASTRO, I.P. 2010 Large-eddy simulation of dispersion from surface sources in arrays of obstacles. *Boundary-Layer Meteorol.* **135** (3), 433–454.

BUSSE, A. & JELLY, T.O. 2020 Influence of surface anisotropy on turbulent flow over irregular roughness. *Flow Turbul. Combust.* **104** (2), 331–354.

BUSSE, A., THAKKAR, M. & SANDHAM, N.D. 2017 Reynolds-number dependence of the near-wall flow over irregular rough surfaces. *J. Fluid Mech.* **810**, 196–224.

BUSSE, A. & ZHDANOV, O. 2022 Direct numerical simulations of turbulent channel flow over ratchet roughness. *Flow Turbul. Combust.* **109** (4), 1195–1213.

CHAN, L., MACDONALD, M., CHUNG, D., HUTCHINS, N. & OOI, A. 2015 A systematic investigation of roughness height and wavelength in turbulent pipe flow in the transitionally rough regime. *J. Fluid Mech.* **771**, 743–777.

CHUNG, D., HUTCHINS, N., SCHULTZ, M.P. & FLACK, K.A. 2021 Predicting the drag of rough surfaces. *Annu. Rev. Fluid Mech.* **53**, 439–471.

DE MARCHIS, M. 2016 Large eddy simulations of roughened channel flows: estimation of the energy losses using the slope of the roughness. *Comput. Fluids* **140**, 148–157.

DE MARCHIS, M., MILICI, B. & NAPOLI, E. 2019 Large eddy simulations on the effect of the irregular roughness shape on turbulent channel flows. *Intl J. Heat Fluid Flow* **80**, 108494.

DE MARCHIS, M., SACCONE, D., MILICI, B. & NAPOLI, E. 2020 Large eddy simulations of rough turbulent channel flows bounded by irregular roughness: advances toward a universal roughness correlation. *Flow Turbul. Combust.* **105** (2), 627–648.

DVORAK, F.A. 1969 Calculation of turbulent boundary layers on rough surfaces in pressure gradient. *AIAA J.* **7** (9), 1752–1759.

FLACK, K.A. & SCHULTZ, M.P. 2010 Review of hydraulic roughness scales in the fully rough regime. *Trans. ASME J. Fluids Engng* **132** (4), 041203.

FLACK, K.A. & SCHULTZ, M.P. 2014 Roughness effects on wall-bounded turbulent flows. *Phys. Fluids* **26** (10), 101305.

FLACK, K.A., SCHULTZ, M.P. & VOLINO, R.J. 2020 The effect of a systematic change in surface roughness skewness on turbulence and drag. *Intl J. Heat Fluid Flow* **85**, 108669.

FOROOGHI, P., STROH, A., MAGAGNATO, F., JAKIRLIĆ, S. & FROHNAPFEL, B. 2017 Toward a universal roughness correlation. *Trans. ASME J. Fluids Engng* **139** (12), 121201.

GATTI, D., VON DEYN, L., FOROOGHI, P. & FROHNAPFEL, B. 2020 Do riblets exhibit fully rough behaviour? *Exp Fluids.* **61** (3), 1–6.

HAMA, F.R. 1954 Boundary layer characteristics for smooth and rough surfaces. *Trans. Soc. Nav. Archit. Mar. Engrs* **62**, 333–358.

HONG, J., KATZ, J. & SCHULTZ, M.P. 2011 Near-wall turbulence statistics and flow structures over three-dimensional roughness in a turbulent channel flow. *J. Fluid Mech.* **667**, 1–37.

JIMÉNEZ, J. 2004 Turbulent flows over rough walls. *Annu. Rev. Fluid Mech.* **36**, 173–196.

LEONARDI, S., ORLANDI, P. & ANTONIA, R.A. 2007 Properties of d- and k-type roughness in a turbulent channel flow. *Phys. Fluids* **19**, 125101.

LEONARDI, S., ORLANDI, P., SMALLEY, R.J., DJENIDI, L. & ANTONIA, R.A. 2003 Direct numerical simulations of turbulent channel flow with transverse square bars on one wall. *J. Fluid Mech.* **491**, 229–238.

MACDONALD, M., CHAN, L., CHUNG, D., HUTCHINS, N. & OOI, A. 2016 Turbulent flow over transitionally rough surfaces with varying roughness densities. *J. Fluid Mech.* **804**, 130–161.

MACDONALD, R.W., GRIFFITHS, R.F. & HALL, D.J. 1998 An improved method for the estimation of surface roughness of obstacle arrays. *Atmos. Environ.* **32** (11), 1857–1864.

MEJIA-ALVAREZ, R. & CHRISTENSEN, K.T. 2013 Wall-parallel stereo particle-image velocimetry measurements in the roughness sublayer of turbulent flow overlying highly irregular roughness. *Phys. Fluids* **25** (11), 115109.

MILLWARD-HOPKINS, J.T., TOMLIN, A.S., MA, L., INGHAM, D. & POURKASHANIAN, M. 2011 Estimating aerodynamic parameters of urban-like surfaces with heterogeneous building heights. *Boundary-Layer Meteorol.* **141**, 443–465.

MODESTI, D., ENDRIKAT, S., HUTCHINS, N. & CHUNG, D. 2021 Dispersive stresses in turbulent flow over riblets. *J. Fluid Mech.* **917**, A55.

NAPOLI, E., ARMENIO, V. & DE MARCHIS, M. 2008 The effect of the slope of irregularly distributed roughness elements on turbulent wall-bounded flows. *J. Fluid Mech.* **613**, 385–394.

NIKURADSE, J. 1933 Laws of flow in rough pipes. *NACA Tech. Mem.* TM 1292 (1950), pp. 1–62.

OKE, T.R. 1988 Street design and urban canopy layer climate. *Energy Build.* **11** (1–3), 103–113.

ORLANDI, P. & LEONARDI, S. 2006 DNS of turbulent channel flows with two- and three-dimensional roughness. *J. Turbul.* (7), N73.

ORLANDI, P. & LEONARDI, S. 2008 Direct numerical simulation of three-dimensional turbulent rough channels: parameterization and flow physics. *J. Fluid Mech.* **606**, 399–415.

PIOMELLI, U. 2019 Recent advances in the numerical simulation of rough-wall boundary layers. *Phys. Chem. Earth* **113**, 63–72.

RAUPACH, M.R., ANTONIA, R.A. & RAJAGOPALAN, S. 1991 Rough-wall turbulent boundary layers. *Appl. Mech. Rev.* **44**, 1–25.

SCHLICHTING, H. 1937 Experimental investigation of surface roughness. *NACA Tech. Mem.* TM 823.

SHAO, Y. & YANG, Y. 2005 A scheme for drag partition over rough surfaces. *Atmos. Environ.* **39** (38), 7351–7361.

SHAO, Y. & YANG, Y. 2008 A theory for drag partition over rough surfaces. *J. Geophys. Res.: Earth* **113** (F2).

SIGAL, A. & DANBERG, J.E. 1990 New correlation of roughness density effect on the turbulent boundary layer. *AIAA J.* **28** (3), 554–556.

THAKKAR, M., BUSSE, A. & SANDHAM, N. 2017 Surface correlations of hydrodynamic drag for transitionally rough engineering surfaces. *J. Turbul.* **18** (2), 138–169.

VAN RIJ, J.A., BELNAP, B.J. & LIGRANI, P.M. 2002 Analysis and experiments on three-dimensional, irregular surface roughness. *Trans. ASME J. Fluids Engng* **124** (3), 671–677.

VOLINO, R.J., SCHULTZ, M.P. & FLACK, K.A. 2011 Turbulence structure in boundary layers over periodic two- and three-dimensional roughness. *J. Fluid Mech.* **676**, 172–190.

WAIGH, D.R. & KIND, R.J. 1998 Improved aerodynamic characterization of regular three-dimensional roughness. *AIAA J.* **36** (6), 1117–1119.

YANG, X.I.A., SADIQUE, J., MITTAL, R. & MENEVEAU, C. 2016 Exponential roughness layer and analytical model for turbulent boundary layer flow over rectangular-prism roughness elements. *J. Fluid Mech.* **789**, 127–165.